

# Chemical Vapor Deposition of Large-Sized Hexagonal WSe<sub>2</sub> Crystals on Dielectric Substrates

Jianyi Chen, Bo Liu, Yanpeng Liu, Wei Tang, Chang Tai Nai, Linjun Li, Jian Zheng, Libo Gao, Yi Zheng, Hyun Suk Shin, Hu Young Jeong, and Kian Ping Loh\*

Transition metal dichalcogenide (TMD) monolayers are the “semiconductor” analogues of graphene. Due to its 2D confinement, they show unique electronic and optical properties which can be exploited to construct heterostructures and applied in light harvesting or photochemical devices.<sup>[1–3]</sup> Monolayer WSe<sub>2</sub> is a direct-gap semiconductor with an optical band gap of  $\gg 1.653$  eV.<sup>[2,4,5]</sup> The p-type transistor behaviors observed in bulk and mechanically exfoliated WSe<sub>2</sub> flakes<sup>[6,7]</sup> complements other 2D materials<sup>[8]</sup> such as gapless semimetal graphene, insulating boron nitride, and n-type semiconductors such as MoS<sub>2</sub>, WS<sub>2</sub>, and MoSe<sub>2</sub> in device heterostructures. Many approaches have been developed to synthesize high-quality monolayer WSe<sub>2</sub>.<sup>[9]</sup> However, micromechanical exfoliation produces small flakes with lateral dimensions in tens of micrometers ( $\mu\text{m}$ ).<sup>[1,10]</sup> WSe<sub>2</sub> have also been grown on sapphire<sup>[11]</sup> and SiO<sub>2</sub> by the chemical vapor deposition (CVD),<sup>[12]</sup> but individual crystallites are typically smaller than 10  $\mu\text{m}$  in width. Recently, polycrystalline WSe<sub>2</sub> films have been deposited on SiO<sub>2</sub> by low-pressure CVD<sup>[13]</sup> but the grains are typically smaller than 5  $\mu\text{m}$ . To date, synthesis of good quality, large-sized WSe<sub>2</sub> crystals on dielectric substrates remains a challenge. It is therefore timely to investigate the conditions for the growth of large-sized WSe<sub>2</sub> crystalline domains, especially since WSe<sub>2</sub> is one of the few p-type 2D complementing the n-type chalcogenide family.

Herein, we demonstrate the growth of large-sized high-quality hexagonal WSe<sub>2</sub> crystals on dielectric substrates such as SiO<sub>2</sub> and Si<sub>3</sub>N<sub>4</sub> by a modified CVD method. Direct deposition of large-sized WSe<sub>2</sub> crystals on low-cost Si<sub>3</sub>N<sub>4</sub> or SiO<sub>2</sub> dielectrics is important because it allows the fabrication of field-effect transistors (FET) where the dielectrics serve as part of the electrical

back gate. The appearance of hexagonal WSe<sub>2</sub> crystals demonstrates the versatility of TMD growth, and enlarges the shape family of WSe<sub>2</sub> crystals. Our growth recipe allows us to tune the shape of the crystals from triangular to hexagonal, with a maximum size of about 168  $\mu\text{m}$ . Raman, transmission electron microscopy (TEM) and FET measurements indicated that the crystals have excellent crystalline and electronic properties.

The CVD growth was performed in a tube furnace with selenium (Se) and tungsten trioxide (WO<sub>3</sub>) as the precursors, which are described in Figure 1a. Typically, WO<sub>3</sub> powder (about 1.0 mg) was placed on dielectric substrates and introduced into the heating zone center of the furnace. A smaller quartz tube, sealed at one end, and containing 1.0 g of Se, was located upstream and the open end exposed to the center of the furnace to allow the diffusion of Se vapor into reaction area. During the heating stage, H<sub>2</sub> first reacts with WO<sub>3</sub> to form volatile WO<sub>3-x</sub> ( $x = 0-3$ ) suboxides. When the temperature at the center of the furnace approached 720 °C, we moved the furnace to set the temperature of Se powders at  $\gg 280$  °C and the temperature of substrates at about 700 °C. After 30 min growth, discrete WSe<sub>2</sub> islands can be formed on the surface of SiO<sub>2</sub>/Si and Si<sub>3</sub>N<sub>4</sub>/SiO<sub>2</sub>/Si substrates (Figure 1b–e). The shape of the crystals can be tuned by the ratio of carrier gas (H<sub>2</sub> and Ar). After exposure to the reaction gas mixture (H<sub>2</sub>:Ar = 2:50 standard cubic centimeters per minute (sccm)), the dielectric surface was covered mainly by triangular WSe<sub>2</sub> crystals (Figure 1b,c). The straight edges suggest that these triangular WSe<sub>2</sub> crystals have uniform edge structure.<sup>[2,14]</sup> Similar to other TMDs,<sup>[14,15]</sup> adjacent WSe<sub>2</sub> can also grow together and formed twin-crystal structure with a ribbon-like or star-like shape (Figure S1, Supporting Information). With increasing H<sub>2</sub> partial pressure, the population of the triangular crystals decreases, and the size of the crystal increases. As the flow-rate ratio of H<sub>2</sub>/Ar increases to 5:50 sccm, we observed the emergence of hexagon-shaped WSe<sub>2</sub> crystals (Figure 1d,e). The hexagonal shape is notably different from the star-like twin crystals (Figure S1, Supporting Information), which suggests a different growth mechanism. Figure 1f shows a size histogram of triangular and hexagonal crystals observed using optical microscopy. The majority of hexagonal crystals synthesized at a higher H<sub>2</sub> partial pressure are larger in size than those produced at a lower H<sub>2</sub> partial pressure. The largest hexagonal crystals have lateral width of 170  $\mu\text{m}$  and area of about 18 000  $\mu\text{m}^2$  (Figure 1g). The area is about 20 times larger than that of triangular WSe<sub>2</sub> crystals,<sup>[3,11–13]</sup> and also larger than that of other TMDs crystals.<sup>[14,15]</sup> The enlarged image (Figure 1h) displays a uniform color contrast on SiO<sub>2</sub>/Si substrate, indicating that these hexagonal crystals are of uniform thickness.

Dr. J. Chen, Dr. B. Liu, Y. Liu, W. Tang, C. T. Nai,  
Dr. L. Li, Dr. J. Zheng, Dr. L. Gao, Dr. Y. Zheng,  
Prof. K. P. Loh

Centre for Advanced 2D Materials  
and Graphene Research Centre  
Department of Chemistry  
National University of Singapore  
6 Science Drive 2, 117546, Singapore  
E-mail: chmlhkp@nus.edu.sg

Prof. H. S. Shin, Prof. H. Y. Jeong  
Department of Chemistry  
Department of Energy Engineering,  
Low Dimensional Carbon Materials Center  
UNIST Central Research Facilities (UCRF)  
and Center for Multidimensional Carbon Materials  
Institute of Basic Science  
Ulsan National Institute of Science and Technology (UNIST)  
UNIST-gil 50, Ulsan 689-798, South Korea



DOI: 10.1002/adma.201503446

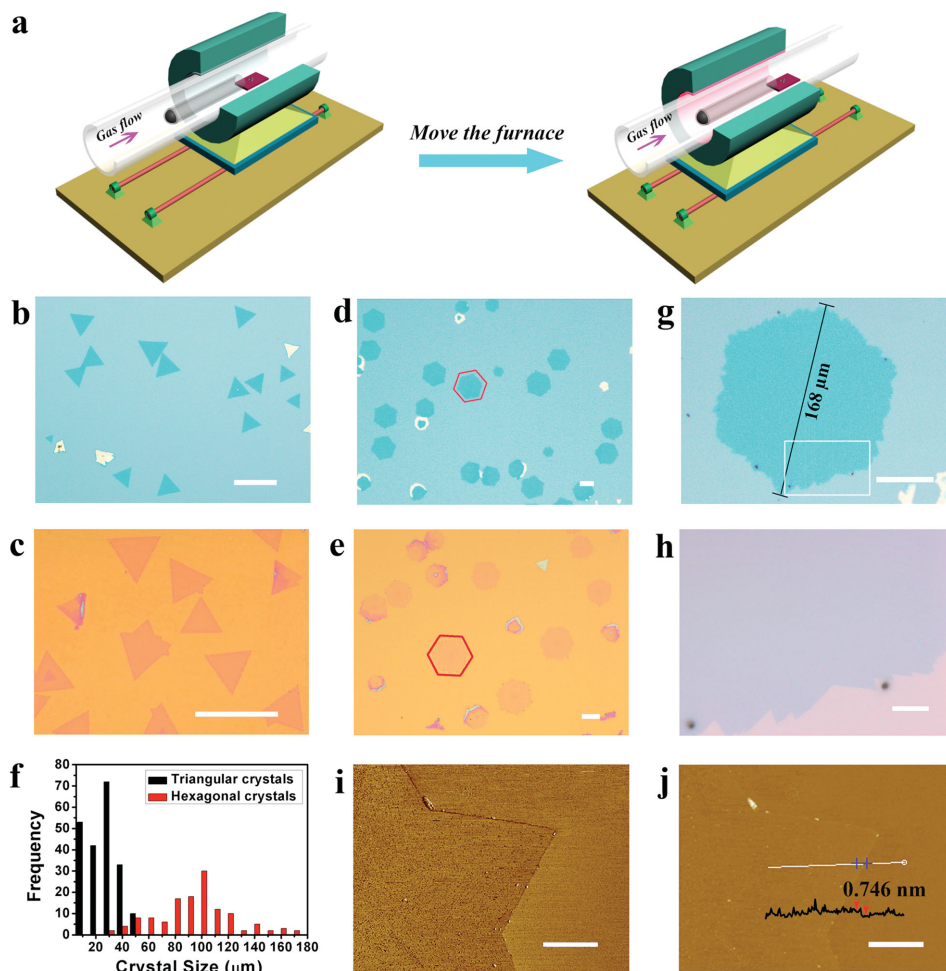


**Figure 1.** a) Schematic diagram of hexagonal WSe<sub>2</sub> growth by using a modified CVD. b,c) Optical images of triangular WSe<sub>2</sub> crystals on SiO<sub>2</sub>/Si (b) and Si<sub>3</sub>N<sub>4</sub>/SiO<sub>2</sub>/Si (c). d,e) Optical images of hexagonal WSe<sub>2</sub> crystals on SiO<sub>2</sub>/Si substrate (d) and Si<sub>3</sub>N<sub>4</sub>/SiO<sub>2</sub>/Si (e). f) Size distribution of triangular and hexagonal crystals obtained at different H<sub>2</sub> flow. g) Optical image of a large-size WSe<sub>2</sub> crystal on SiO<sub>2</sub>/Si. Scale bar 50 μm. h) Zoom-in view of the region outlined by the rectangle in (g). i,j) AFM height (i) and phase (j) images of WSe<sub>2</sub> crystals on SiO<sub>2</sub>/Si substrate. Scale bar is 2 μm.

Atomic force microscopy (AFM) images of a WSe<sub>2</sub> crystal grown on SiO<sub>2</sub>/Si surface are shown in Figure 1i,j. The phase image (Figure 1i) reveals a clear contrast with the SiO<sub>2</sub>/Si substrate and the thickness of the WSe<sub>2</sub> sheet is about 0.746 nm (Figure 1j), corresponding to monolayer WSe<sub>2</sub>. The edges of the hexagonal WSe<sub>2</sub> crystals were examined using AFM. All of the edges have jagged morphology (Figure S2, Supporting Information), which suggests a diffusion-limited growth kinetics.<sup>[16]</sup> Interestingly, the edges are decorated by tiny saw tooth which reveals 60° and 120° corners. The appearance of 120° corners suggests the coexistence of W-edge and Se-edge according to the structure of MoS<sub>2</sub> nanocrystals.<sup>[17]</sup>

The micro-structure and chemical composition of the WSe<sub>2</sub> crystals were probed by TEM, selected area electron diffraction (SAED), energy dispersive spectroscopy (EDS), and X-ray photoemission spectroscopy (XPS). The WSe<sub>2</sub> samples were transferred onto a copper grid using the typical PMMA transfer technique.<sup>[18]</sup> In Figure 2a, a low magnification TEM image shows the film-like structure, and the corresponding SAED pattern (Figure 2b) reveals the hexagonal lattice.<sup>[11,13]</sup> The clear

sixfold diffraction spots indicate that the sample is single crystalline. EDS (Figure 2c) reveals that the atomic ratio between W and Se is about 1:2, which is indicative of stoichiometric WSe<sub>2</sub>. Figure 2d,f shows the high-resolution TEM images of the WSe<sub>2</sub> sample. The surface is clean (Figure 2d) and the edge of the image (Figure 2e) indicates that the film is monolayer. The clear atomic structure (Figure 2f) demonstrates that the CVD WSe<sub>2</sub> crystals are highly crystalline.

XPS was used to measure the binding energies of the W and Se of WSe<sub>2</sub> samples on SiO<sub>2</sub>/Si substrate. The binding energies for the W 4f<sub>7/2</sub> and W 4f<sub>5/2</sub> (Figure 2g) doublets are located at 33.4 and 35.5 eV, and the binding energies for the Se 3d<sub>5/2</sub> and Se 3d<sub>3/2</sub> (Figure 2h) doublets are located at 55.7 and 56.6 eV, respectively, which is consistent with the reported values for WSe<sub>2</sub>.<sup>[19,20]</sup> Survey scan XPS spectrum (Figure S3, Supporting Information) reveals that the sample has high chemical purity, indicating the direct synthesis of WSe<sub>2</sub> crystals on SiO<sub>2</sub> substrates.

Figure 3a–f shows the Raman and photoluminescence (PL) spectra of hexagonal WSe<sub>2</sub> crystals recorded using a laser

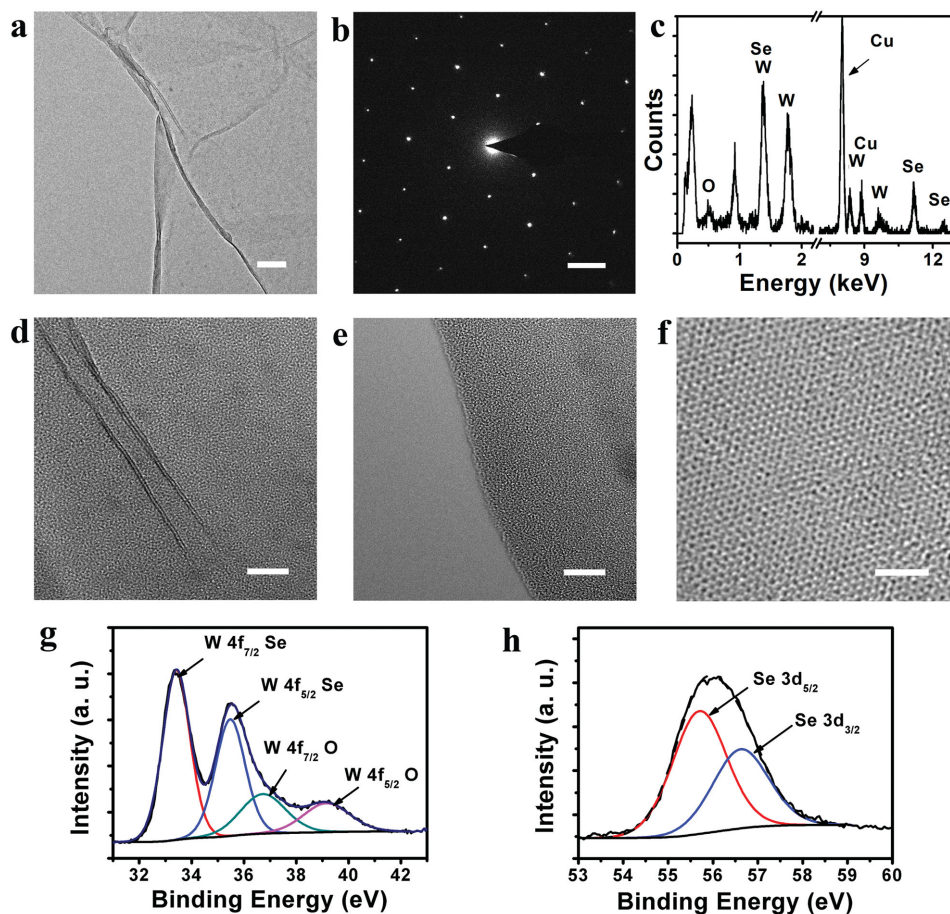


**Figure 2.** a) Low magnification TEM image of WSe<sub>2</sub> crystal. Scale bar 100 nm. b) Hexagonal SAED pattern of the crystal. c) EDX analysis. d–f) High-resolution TEM images of WSe<sub>2</sub>. Scale bar 10 nm in (d,e) and 2 nm in (f). g,h) XPS spectra of WSe<sub>2</sub> crystals showing W 4f (g) and Se 3d (h).

excitation of 532 nm. The Raman and PL mapping signals were extracted from the integrated intensities of the characteristic WSe<sub>2</sub> Raman peaks at E<sub>1g</sub><sup>1</sup> mode ( $\approx 248$  cm<sup>-1</sup>) and PL emission ( $\approx 760$  nm), and their spatial dependences are plotted in Figure 3a,b for a single WSe<sub>2</sub> grain grown on SiO<sub>2</sub> substrate and in Figure 3c,d for a single WSe<sub>2</sub> grain on Si<sub>3</sub>N<sub>4</sub>. Intensity mapping provides an assessment of the thickness uniformity of the sample. The uniform color intensity observed suggest that the monolayer WSe<sub>2</sub> domains on SiO<sub>2</sub> and Si<sub>3</sub>N<sub>4</sub> substrates are uniform in thickness. On both substrates, Raman spectra (Figure 3e) reveal two characteristic peaks at 248 and 259 cm<sup>-1</sup>, which are assignable to the E<sub>1g</sub><sup>1</sup> and A<sub>1g</sub> mode, respectively.<sup>[11,21]</sup> Two high-energy bands at 358 and 374 cm<sup>-1</sup> are also identified, which are attributed to the 2E<sub>1g</sub> and A<sub>1g</sub> + LA modes.<sup>[11,22]</sup> All of these peaks agree well with that of the exfoliated monolayer samples.<sup>[21,22]</sup> The PL spectra of the crystals (Figure 3f) exhibit strong emission at  $>760$  nm, corresponding to the direct band gap at K point.<sup>[23]</sup> The full-half-maximum (FWHM) value is about 25 nm, in agreement with previously reported values for exfoliated WSe<sub>2</sub>.<sup>[21]</sup> The PL peak of the crystals on Si<sub>3</sub>N<sub>4</sub> displays a slight red-shift compared with that on SiO<sub>2</sub> probably due to the different interaction between WSe<sub>2</sub> and substrates. Nevertheless, all the crystals display strong PL signal, which are evident of highly crystalline, monolayer quality.

To assess the generality of our method for growing other 2D TMDs hexagonal crystals, hexagonal MoSe<sub>2</sub> crystals were synthesized using a similar strategy. MoSe<sub>2</sub> were grown using MoO<sub>3</sub>, Se powders and H<sub>2</sub> as the source precursors, with H<sub>2</sub> gas first reacting with MoO<sub>3</sub> to form MoO<sub>3-x</sub> ( $x = 1-3$ ), followed by the introduction of Se for successive growth of MoSe<sub>2</sub> crystals. Under suitable conditions, hexagonal MoSe<sub>2</sub> crystals can be grown on SiO<sub>2</sub>/Si substrates (Figure 3g). Due to the higher volatility of MoO<sub>3</sub>, the quantity of MoSe<sub>2</sub> crystals obtained is more than that of WSe<sub>2</sub> crystals. The thickness of a MoSe<sub>2</sub> crystal measured by AFM (Figure 3h) is about 0.620 nm. The Raman spectrum shows characteristic resonance peaks of monolayer MoSe<sub>2</sub> (Figure 3i),<sup>[24]</sup> with the out-of-plane A<sub>1g</sub> mode at  $\approx 239$  cm<sup>-1</sup> and the in-plane E<sub>2g</sub> mode at  $\approx 286$  cm<sup>-1</sup>. The PL spectrum (inset) shows the characteristic emission peak corresponding to the emission of monolayer MoSe<sub>2</sub> (793 nm).<sup>[24]</sup> These results indicate these hexagonal crystals are monolayer MoSe<sub>2</sub> with perfect optical properties.

It has been proposed that the CVD growth of TMDs occurs by a solid–vapor–solid mechanism.<sup>[25]</sup> The growth of WSe<sub>2</sub> (similar to MoSe<sub>2</sub>) crystals on dielectric substrates involves the reaction between Se, WO<sub>3</sub>, and H<sub>2</sub>.<sup>[11-13]</sup> At elevated temperature, WO<sub>3</sub> powder was reduced by H<sub>2</sub> to form volatile WO<sub>3-x</sub> suboxides. These suboxides diffused outward and further

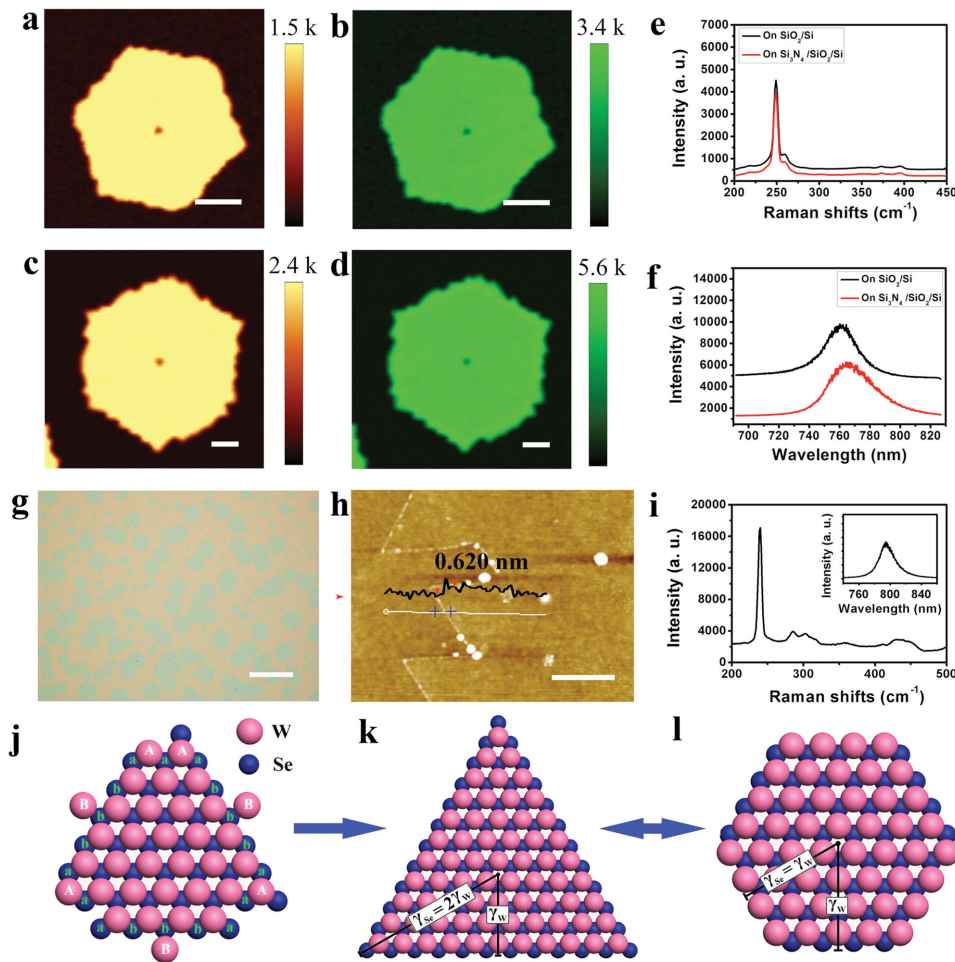


**Figure 3.** a,b) Raman (a) and PL mapping (b) of a monolayer WSe<sub>2</sub> crystal on SiO<sub>2</sub>/Si. Scale bar 20 μm. c,d) Raman (c) and PL mapping (d) of a monolayer WSe<sub>2</sub> crystal on Si<sub>3</sub>N<sub>4</sub>/SiO<sub>2</sub>/Si. Scale bar 10 μm. e) Raman spectrum of monolayer WSe<sub>2</sub> crystals. f) PL spectrum of monolayer WSe<sub>2</sub> crystals. g) Optical image of hexagonal MoSe<sub>2</sub> grown on SiO<sub>2</sub>/Si substrate. Scale bar 100 μm. h) AFM image of a typical MoSe<sub>2</sub> crystal. Scale bar 500 nm. i) Raman spectra of monolayer MoSe<sub>2</sub>. The inset shows the PL spectrum. j) Atomic ball model illustrating the rapid growth of W edges under enough Se supply. Green “a” and “b” atoms is the Se atoms that bonded at W-edges and Se-edges respectively. Green “A” and “B” atoms is the W atoms that would bond with the Se atoms at W-edges and Se-edges, respectively. k,l) Atomic ball model of triangular and hexagonal WSe<sub>2</sub> crystals. If  $\gamma_{Se} > 2 \times \gamma_W$  the crystal shows a triangular morphology terminated exclusively by W edge, or vice versa terminated by Se edge. Intermediate values result in crystals with a hexagonal symmetry.

reacted with Se to form WSe<sub>2</sub> nucleation points. The competing reactions of Se and WO<sub>3-x</sub> at the edges of these WSe<sub>2</sub> nucleation points determine the shape of WSe<sub>2</sub> crystals (Figure 3j). At a low H<sub>2</sub> concentration, the quantity of active WO<sub>3-x</sub> generated is lower relative to Se vapor, thus Se reacts with and consumes the W edges. However, WO<sub>3-x</sub> deposits W atoms onto Se atoms at Se edges and W edges selectively. Compared with Se edges, the reaction at the W edges is more rapid. Therefore, continuous fast growth at the W edges will cause the disappearance of W edges, resulting in the formation of triangular WSe<sub>2</sub> crystals with three Se edges.<sup>[2]</sup> However, with increasing concentration of H<sub>2</sub>, the quantity of volatilized WO<sub>3-x</sub> increases. The reaction at Se edges is enhanced, and the selected edge growth is weakened accordingly. In terms of a simple Wulff construction,<sup>[26,27]</sup> the shape of the WSe<sub>2</sub> clusters can be expressed as a function of the relative edge free energy of Se edges ( $\gamma_{Se}$ ) and W edge ( $\gamma_W$ ). Triangular crystals occurs when  $\gamma_{Se}/\gamma_W > 2$  or  $\gamma_{Se}/\gamma_W < 0.5$  and

hexagonal crystals occurs when  $0.5 < \gamma_{Se}/\gamma_W < 2$ . By controlling H<sub>2</sub> pressure to produce appropriate fluxes of WO<sub>3-x</sub> and Se, it is possible to achieve a  $\gamma_{Se}/\gamma_W$  value in the range of 0.5–2, which results in the growth of hexagonal WSe<sub>2</sub> crystals on dielectric substrates. Note that, with increasing size of the WSe<sub>2</sub> crystals, the growth of the edges becomes diffusion-limited,<sup>[16]</sup> leading to nonoptimal structure, i.e., jagged edges (Figure S2, Supporting Information). A systematic study of the edge diffusion and the kinetics-limited growth dynamics is still ongoing.

To evaluate the electronic properties of the hexagonal WSe<sub>2</sub> crystals, a series of back-gated FETs (Figure 4a) were fabricated on WSe<sub>2</sub> crystals grown on Si<sub>3</sub>N<sub>4</sub>/SiO<sub>2</sub>/Si (Si<sub>3</sub>N<sub>4</sub>:SiO<sub>2</sub> = 100:300 nm) substrates using graphene as source/drain (S/D) electrodes, with Pd contacting it, via precise transfer technique and electron beam lithography (EBL). Murata et al.<sup>[28]</sup> studied the work function of CVD graphene on Pd using in situ low-energy electron microscopy (LEEM) and density functional

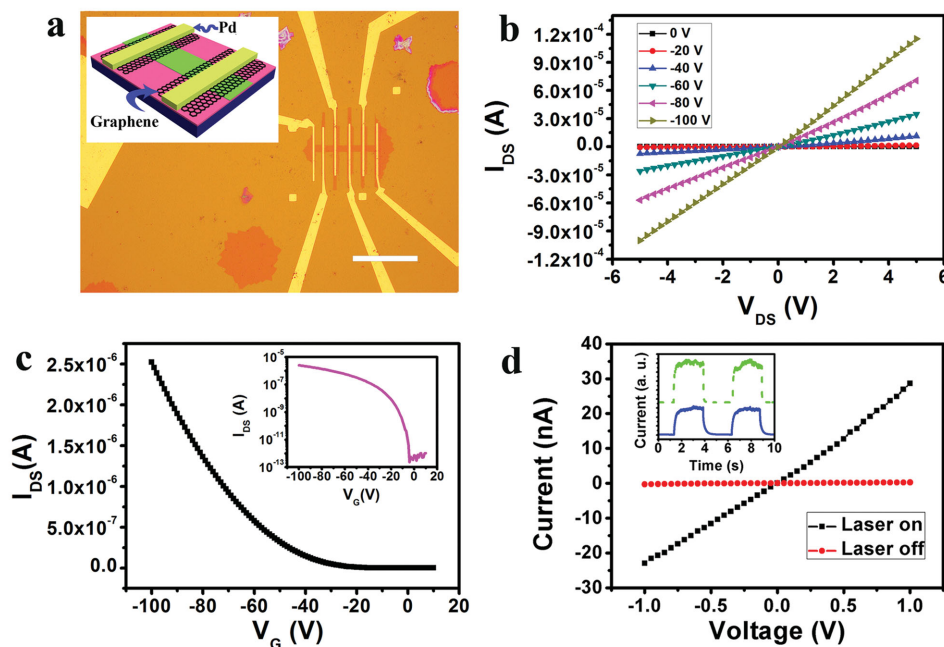


**Figure 4.** a) Optical image of WSe<sub>2</sub> devices using graphene as contact electrodes. Scale bar 100  $\mu$ m. The inset shows a schematic diagram of this device. b) Current ( $I_{DS}$ )/voltage ( $V_{DS}$ ) curves for a device with a channel length  $L \gg 10 \mu$ m and channel width  $W \gg 10 \mu$ m in N<sub>2</sub>. As the gate voltage is varied from 0 to -100 V, the conductance of the device increases, which is indicative of p-type behavior. c) Transfer curves of current ( $I_{DS}$ ) versus gate voltage ( $V_G$ ) of the WSe<sub>2</sub> device at  $V_{DS} = 0.1$  V in N<sub>2</sub>. The inset shows the logarithmic value of  $I_{DS}$  as a function of  $V_G$ , indicative of a high on/off current ratio. d) Dependence of current on source–drain voltage with and without laser illumination. The inset shows photoresponsivity of the devices using graphene (dashed green line) and Pd (solid blue line) as electrodes. The introduction of graphene have effectively removed residual conductivity.

theory (DT) calculations, and reported that graphene-covered Pd has a work function of  $4.3 \pm 0.1$  eV. The matching work function with WSe<sub>2</sub> ( $>4.3$  eV for WSe<sub>2</sub><sup>[29]</sup>) and the excellent 2D interface contact reduces the metal–WSe<sub>2</sub> Schottky barrier, and facilitate carrier injection in the devices. Figure 4b demonstrates the output characteristics (drain current  $I_{DS}$  vs drain voltage  $V_{DS}$ ) of a typical device with a channel width and length of 10  $\mu$ m, respectively, measured in an inert atmosphere of N<sub>2</sub>. It displays a linear increase of the drain current ( $I_{DS}$ ) with negative drain voltage ( $V_{DS}$ ), indicating that Ohmic contacts were formed at the source and drain electrodes. The transfer characteristic of the device is illustrated in Figure 4c, which exhibits a typical p-type characteristic with a high on/off current ratio of  $10^6$ . Field-effect mobility of holes can be extracted based on the slope  $\Delta I_{DS}/\Delta V_G$  fitted to the linear regime of the transfer curves. The FET mobilities of our devices are in the range of 1–100 cm<sup>2</sup> V<sup>-1</sup> s<sup>-1</sup>, comparable to those of exfoliated flakes and CVD synthetic crystals.<sup>[3,11]</sup>

To further confirm the good electrical contact between 2D graphene and WSe<sub>2</sub>, we also measured the photoelectrical properties of the device (Figure 4d). When illuminated using a 532 nm laser (power 0.5 mW, spot size  $\approx 2$  mm<sup>2</sup>), photocurrent current with an on-off ratio of  $\approx 10^2$  can be obtained at 1 V. The photoresponsivity ( $R$ ) is calculated to be  $\approx 1100$  mA W<sup>-1</sup> in ambient air,<sup>[30]</sup> which is higher than that of other WSe<sub>2</sub> photodetectors.<sup>[31,32]</sup> The on–off pulses are well defined (inset), indicating that contact resistance is low due to the presence of graphene-interlayer.

In summary, we report the CVD of monolayer hexagonal WSe<sub>2</sub> crystals on dielectric substrates such as SiO<sub>2</sub> and Si<sub>3</sub>N<sub>4</sub>.

Introducing H<sub>2</sub>, and adjusting its partial pressure, allows us to produce isolated, monolayer WSe<sub>2</sub> crystals in which the shapes can be controlled. Our work provides an effective method for synthesizing large-sized hexagonally shaped WSe<sub>2</sub> crystals. FET devices fabricated on individual hexagonal WSe<sub>2</sub> crystal using graphene electrode display a maximum hole mobility of about 100 cm<sup>2</sup> V<sup>-1</sup> s<sup>-1</sup> with a high photoresponsivity of  $\approx 1100$  mA W<sup>-1</sup> due to perfect contact between graphene and WSe<sub>2</sub>. The ability to directly synthesize large-sized high-quality hexagonal TMD crystals on dielectric substrates is important for basic research and practical applications.

## Experimental Section

**Preparation of WSe<sub>2</sub> Crystals:** WSe<sub>2</sub> crystals were grown on dielectric substrates by using atmospheric pressure CVD. The growth substrates such as SiO<sub>2</sub>/Si and Si<sub>3</sub>N<sub>4</sub>/SiO<sub>2</sub>/Si were cleaned in acetone, isopropanol, and water, followed by 10 min of O<sub>2</sub> plasma. A little WO<sub>3</sub> powder (about 1.0 mg) was placed on growth substrates, and located them in the heating zone center of the furnace. A quartz tube with one end sealed containing 1.0 g of selenium was located upstream as a source for the selenylation of WO<sub>3</sub>. 5 H<sub>2</sub> and 50 sccm Ar was used as carrier gas during the CVD process. The furnace was heated to 720  $^{\circ}$ C. As the temperature at the center of the furnace approached 720  $^{\circ}$ C, the furnace was moved to make the temperature of Se powders at  $\approx 280$   $^{\circ}$ C and the temperature of substrates at about 700  $^{\circ}$ C. After stabilizing the system for 30 min, the furnace was naturally cooled. Then the samples were annealed at 350  $^{\circ}$ C under vacuum for 3 h to remove some impurities absorbed on the surface of the samples.

**Characterization:** AFM images were obtained using a Bruker Dimension FastScan Atomic Force Microscope in the tapping mode.

Optical images were obtained using an Olympus BX51 microscopy. TEM was performed with FEI Titan transmission electron microscope operated at 80 kV. Raman spectra were recorded at room temperature using a WITec Raman Microscope with laser excitation at 532 nm.

**Device and Electrical Measurements:** FETs were fabricated on  $\text{Si}_3\text{N}_4/\text{SiO}_2/\text{Si}$  wafers ( $\text{Si}_3\text{N}_4:\text{SiO}_2 = 100:300$  nm) by using EBL technique with graphene as source–drain electrodes and the doped silicon substrate as the back gate. First, single-layer graphene ribbon array etched by EBL was transferred onto a hexagonal  $\text{WSe}_2$  crystal by using precise transfer technique. Then Pd electrodes were fabricated on graphene ribbons by EBL technique and thermal evaporation. Finally, the  $\text{WSe}_2$  in the channel was etched into ribbons by EBL technique. The metal electrodes had a thickness of 50 nm. The FET characteristics were measured in  $\text{N}_2$  at room temperature. A Keithley 4200SC semiconductor parameter analyzer was used to measure the electrical characteristics of the devices. The photoelectrical properties of the device was measured in ambient air. The device is illuminated using a 532 nm laser. The power of the laser is about 0.5 mW with a spot size of  $\approx 2$  mm<sup>2</sup>.

## Supporting Information

Supporting Information is available from the Wiley Online Library or from the author.

## Acknowledgements

J.C., B.L., and Y.L. contributed equally to this work and K.P.L. supervised it. The authors acknowledge support by National Research Foundation Competitive Research Programs: 1. NRF-CRP 001–123:Control of exotic quantum phenomena at strategic interfaces and surfaces for novel functionality by in situ Synchrotron radiation and 2. Novel 2D Materials with Tailored Properties: Beyond Graphene R-143–000–295–281. J.C. designed and performed the experiments and wrote the manuscript with K.P.L.

Received: July 17, 2015

Revised: August 1, 2015

Published online: September 28, 2015

- [1] C. H. Lee, G. H. Lee, A. M. van der Zande, W. Chen, Y. Li, M. Han, X. Cui, G. Arefe, C. Nuckolls, T. F. Heinz, J. Guo, J. Hone, P. Kim, *Nat. Nanotechnol.* **2014**, *9*, 676.
- [2] C. Huang, S. Wu, A. M. Sanchez, J. J. P. Peters, R. Beanland, J. S. Ross, P. Rivera, W. Yao, D. H. Cobden, X. Xu, *Nat. Mater.* **2014**, *13*, 1096.
- [3] X. Duan, C. Wang, J. C. Shaw, R. Cheng, Y. Chen, H. Li, X. Wu, Y. Tang, Q. Zhang, A. Pan, J. Jiang, R. Yu, Y. Huang, X. Duan, *Nat. Nanotechnol.* **2014**, *9*, 1024.
- [4] L. H. Brixner, *J. Inorg. Nucl. Chem.* **1962**, *24*, 257.
- [5] M. M. Ugeda, A. J. Bradley, S. F. Shi, F. H. da Jornada, Y. Zhang, D. Y. Qiu, W. Ruan, S. K. Mo, Z. Hussain, Z. X. Shen, F. Wang, S. G. Louie, M. F. Crommie, *Nat. Mater.* **2014**, *13*, 1091.
- [6] H. Fang, S. Chuang, T. C. Chang, K. Takei, T. Takahashi, A. Javey, *Nano Lett.* **2012**, *12*, 3788.
- [7] V. Podzorov, M. E. Gershenson, C. Kloc, R. Zeis, E. Bucher, *Appl. Phys. Lett.* **2004**, *84*, 3301.
- [8] A. K. Geim, I. V. Grigorieva, *Nature* **2013**, *499*, 419.
- [9] M. Chhowalla, H. S. Shin, G. Eda, L. J. Li, K. P. Loh, H. Zhang, *Nat. Chem.* **2013**, *5*, 263.
- [10] A. Pospischil, M. M. Furchi, T. Mueller, *Nat. Nanotechnol.* **2014**, *9*, 257.
- [11] J. K. Huang, J. Pu, C. L. Hsu, M. H. Chiu, Z. Y. Juang, Y. H. Chang, W. H. Chang, Y. Iwasa, T. Takenobu, L. J. Li, *ACS Nano* **2014**, *8*, 923.
- [12] B. Liu, M. Fathi, L. Chen, A. Abbas, Y. Ma, C. Zhou, *ACS Nano* **2015**, *9*, 6119.
- [13] H. Zhou, C. Wang, J. C. Shaw, R. Cheng, Y. Chen, X. Huang, Y. Liu, N. O. Weiss, Z. Lin, Y. Huang, X. Duan, *Nano Lett.* **2015**, *15*, 709.
- [14] A. M. van der Zande, P. Y. Huang, D. A. Chenet, T. C. Berkelbach, Y. M. You, G. H. Lee, T. F. Heinz, D. R. Reichman, D. A. Muller, J. C. Hone, *Nat. Mater.* **2013**, *12*, 554.
- [15] S. Najmaei, Z. Liu, W. Zhou, X. Zou, G. Shi, S. Lei, B. I. Yakobson, J. C. Idrobo, P. M. Ajayan, J. Lou, *Nat. Mater.* **2013**, *12*, 754.
- [16] M. Einax, W. Dieterich, P. Maass, *Rev. Mod. Phys.* **2013**, *85*, 921.
- [17] J. V. Lauritsen, J. Kibsgaard, S. Helveg, H. Topsøe, B. S. Clausen, E. Lægsgaard, F. Besenbacher, *Nat. Nanotechnol.* **2007**, *2*, 53.
- [18] Y. C. Liu, W. Zhang, J. K. Huang, K. K. Liu, Y. H. Lee, C. T. Liang, C. W. Chu, L. J. Li, *Nanoscale* **2012**, *4*, 6637.
- [19] G. Salitra, G. Hodes, E. Klein, R. Tenne, *Thin Solid Films* **1994**, *245*, 180.
- [20] H. Wang, D. Kong, P. Johanes, J. J. Cha, G. Zheng, K. Yan, N. Liu, Y. Cui, *Nano Lett.* **2013**, *13*, 3426.
- [21] H. Li, G. Lu, Y. Wang, Z. Yin, C. Cong, Q. He, L. Wang, F. Ding, T. Yu, H. Zhang, *Small* **2013**, *9*, 1974.
- [22] W. Zhao, Z. Ghorannevis, A. K. Kumar, J. R. Pang, M. Toh, X. Zhang, C. Kloc, P. H. Tan, G. Eda, *Nanoscale* **2013**, *5*, 9677.
- [23] P. Tonndorf, R. Schmidt, P. Böttger, X. Zhang, J. Börner, A. Liebig, M. Albrecht, C. Kloc, O. Gordan, D. R. T. Zahn, S. M. de Vasconcelos, R. Bratschitsch, *Opt. Express* **2013**, *21*, 4908.
- [24] X. Lu, M. I. B. Utama, J. Lin, X. Gong, J. Zhang, Y. Zhao, S. T. Pantelides, J. Wang, Z. Dong, Z. Liu, W. Zhou, Q. Xiong, *Nano Lett.* **2014**, *14*, 2419.
- [25] S. Wu, C. Huang, G. Aivazian, J. S. Ross, D. H. Cobden, X. Xu, *ACS Nano* **2013**, *7*, 2768.
- [26] G. Wulff, *Z. Kristallogr.* **1901**, *34*, 449.
- [27] J. V. Lauritsen, M. V. Bollinger, E. Lægsgaard, K. W. Jacobsen, J. K. Nørskov, B. S. Clausen, H. Topsøe, F. Besenbacher, *J. Catal.* **2004**, *221*, 510.
- [28] Y. Murata, E. Starodub, B. B. Kappes, C. V. Ciobanu, N. C. Bartelt, K. F. McCarty, S. Kodambaka, *Appl. Phys. Lett.* **2010**, *97*, 143114.
- [29] L. Britnell, R. M. Ribeiro, A. Eckmann, R. Jalil, B. D. Belle, A. Mishchenko, Y. J. Kim, R. V. Gorbachev, T. Georgiou, S. V. Morozov, A. N. Grigorenko, A. K. Geim, C. Casiraghi, A. H. C. Neto, K. S. Novoselov, *Science* **2013**, *340*, 1311.
- [30] W. Zhang, J. K. Huang, C. H. Chen, Y. H. Chang, Y. J. Cheng, L. J. Li, *Adv. Mater.* **2013**, *25*, 3456.
- [31] B. W. H. Baugher, H. O. H. Churchill, Y. Yang, P. Jarillo-Herrero, *Nat. Nanotechnol.* **2014**, *9*, 262.
- [32] J. S. Ross, P. Klement, A. M. Jones, N. J. Ghimire, J. Yan, D. G. Mandrus, T. Taniguchi, K. Watanabe, K. Kitamura, W. Yao, D. H. Cobden, X. Xu, *Nat. Nanotechnol.* **2014**, *9*, 268.